Swelling behavior of butyl and chloroprene rubber composites with poly (sodium acrylate) showing high water-uptake

doi: 10.1002/app.48535

Swelling behavior of butyl and chloroprene rubber composites with poly(sodium acrylate) showing high water-uptake

Yuya Oyama,[1,2] Yusuke Hiejima,[2] Koh-hei Nitta[2]

[1]YKK AP R&D Center, 1, Ogyu, Kurobe, Toyama. 938-8612, Japan

[2]Department of Chemical and Materials Science, Kanazawa University, Kakuma Campus, Kanazawa 920-1192, Japan

Correspondence to: Yusuke Hiejima (E-mail: *hiejima@se.kanazawa-u.ac.jp*)

ABSTRACT

Water-swellable rubber (WSR) comprises super absorbent polymer (SAP) embedded in a rubber matrix and has been commonly used as sealants and caulks, in which high water-uptake and sufficient mechanical strength are required. In this work, we investigated the swelling behavior and mechanical properties of rubber composites comprising SAP powders. A reinforcement effect is caused by the SAP particles, which are described using a modified Guth–Gold equation up to the semi-dilute region. The complex modulus shows upper deviation at high SAP content owing to network formation between SAP particles. The swelling force of the WSR is explained by the amount of SAP particles in the surface layer of the matrix up to the semi-dilute region. The formation of the SAP network leads to an appreciable increase in the swelling force of WSR, as SAP particles embedded in the matrix also contribute to the swelling of WSR.

INTRODUCTION

Water-swellable rubber (WSR) is an elastomeric material with low modulus and high elasticity limit equipped by high water-uptake.[1] WSR materials are commonly fabricated from the blending of super absorbent polymer (SAP) powders into various elastomers, such as chloroprene,[2,3] natural,[4,5] chlorohydrin,[6–8] ethylene propylene diene monomer (EPDM)[9], and styrene-butadiene rubbers.[10] Hydrophilic polymers, such as poly(sodium acrylate) are commonly used as the SAP after the slight cross-linking process to insolubidize it in water.[11] A large amount of water is absorbed when it contacts on WSR, which swells up as SAP can

absorb huge amount of water up to 100 times of its weight. Moreover, the swollen SAP particles form a stable hydrogel, which traps the absorbed water even under external stress. The excellent swelling properties make WSR be utilized as the sealants and caulks in various fields, such as construction of subways and undersea tunnels to prevent water leakage from the junction of concrete walls.[11–16]

The absorption mechanism of SAP[11,13] is explained as follows: When water is added to the SAP, its ionic groups are dissociated, forming a free metal cation (e.g. Na^+) and a polymer pendant anion (e.g. COO^-). The osmotic pressure increases with ionic concentration, resulting in the penetration of water into the polymer matrix. Polymer chains, afterwards, swell due to the coulombic repulsion of the anionic groups, and the SAP can hold a huge amount of hydrated water molecules in the network cavity. The uptake of water is completed when the equilibrium of the osmotic pressure, the hydrophilic affinity, and the elastic stress is attained. While acrylonitrile-grafted starch and modified cellulose were intensively investigated, poly(acrylic acid)-based SAP has recently attracted more interests owing to its high water uptake, low cost, and facile mass production.[2,5,11,17]

The increase of water uptake in the WSR, as well as the improvement of mechanical properties have also been investigated. The discrepancy in polarity between hydrophobic rubber and hydrophilic SAP leads to lower strength due to the aggregation and/or ejection of SAP particles in the matrix rubber, accompanied by the reduction of water uptake. The addition of amphiphilic copolymers and modification of SAP by copolymerization have been investigated to improve the affinity between rubber and SAP.[4,8,17] The addition of carbon black filler effectively prevents the ejection of SAP particles as it results in the formation of a cross-linked structure.[5] The addition of hydrophilic silica as the filler and/or blending of water-

soluble poly(ethylene oxide) improve the rate of water uptake, as it promotes the water penetration into the matrix.[2,3] Although the vulcanization of rubber results in its higher strength, the water uptake is reduced.[18] Furthermore, foaming of WSR, which provides water channels in the matrix, increases the water uptake by two to six times.[9]

Regarding the mechanism of water uptake by WSR, water molecules on the WSR surface are involved into the network structure of the rubbers through the capillary effects and hydrogen bonding to the surface of the SAP particles, followed by the absorption of the SAP embedded in the rubber network.[4,11] Although the absorption of water by SAP particles has already been investigated, regarding the swelling behavior and the rate of water uptake,[19] the mechanism of those embedded in the rubber matrix is still unclear due to the interplay between penetration water into the WSR and swelling of the SAP particles.

The efficiency of water uptake has been evaluated by the increase of the WSR weight compared to its dried weight. The weight of the WSR specimen, which is immersed in water, is measured, even though this method is not suitable for examining water uptake in the early stage, as a short interval is required to observe the rapid increase of the WSR weight. Moreover, the swelling of WSR during its applications (e.g. as sealants and caulks) occurs under a confined geometry, as WSR is usually filled in connectors and fittings. It is important, therefore, to understand the swelling behavior of WSR under confinement, however, the precedent studies are focused on swelling of WSR in free space.

In this work, WSR was fabricated by kneading poly(sodium acrylate) particles into rubbers, and its mechanical properties and morphology were investigated. Meanwhile, the temporal change of the swelling force of WSR filled in a cylinder was monitored, the effects of the shape

of the WSR specimen and content of the SAP were examined, and the mechanism of swelling of WSR under confinement is discussed.

EXPERIMENTAL

Butyl rubber (referred as butyl, degree of unsaturation: 2.3 mol%, mooney viscosity: 33 ML_{1+8}(125 °C), specific gravity: 0.92 g/cm^3) was manufactured by the JSR Corporation, Japan. Polychloroprene rubber (referred as CR, Mooney viscosity: 32-37 ML_{1+4}(100 °C), specific gravity: 1.24 g/cm^3) was obtained from Showa Denko K.K., Japan. Poly(sodium acrylate) particles (referred as SAP, average particle diameter: 30 μm, water absorptivity: 600 g/g) was obtained from Sanyo Chemical Industries, Ltd., Japan.

The SAP particles and the rubber were kneaded with a two-roll mill (6NR-410, Otake Kikai Kougyou K.K, Tokyo, Japan). The rubber (butyl or CR) was first placed in the two-roll mill and masticated for 10 min at 50 °C. Afterwards, the SAP particles were added, and the sample was kneaded for 3 min at 80 °C. The concentrations of SAP samples were 0, 10, 20, 30, 50, and 100 phr. The sheets of the blended materials were prepared by a hot press method and the samples were preheated at 100 °C for 10 min and compressed up to 20 MPa. The samples were kept under the condition for 5 min, and afterwards the pressure was released and they were cooled down to room temperature. The thicknesses of the sample sheets were approximately 0.7, 1.0, and 2.0 mm and WSR specimens with diameters of 10, 20, and 30 mm were cut out from the molded sheets (Table 1).

Differential scanning calorimetry (DSC) was conducted from -60 to 150 °C at a heating rate of 20 °C/min. No clear peak was observed up to 150 °C, indicating that degradation of the sample during the preparation can be neglected.

The morphology of the SAP particles in the WSR was observed by using a microscope (VHX-6000, Keyence, Osaka, Japan). Tensile tests of the dumbbell-shaped specimens (JIS K 6251)

were performed by using the INSTRON tensile machine model 4466 at room temperature and with a crosshead speed of 10 mm/min. Assuming that the volume of specimens is conserved during the tensile test, we used the following equation to convert the true stress σ_t from the nominal stress σ:

$$\sigma_t = \sigma\lambda, \quad (1)$$

where λ is the extension ratio. A dynamic mechanical analysis (DMA) was executed by using the DVE-V4 (UBM, Kyoto, Japan) with sample dimensions of 20 mm × 4 mm × 1 mm. The storage and loss moduli and tanδ were measured at a frequency of 10 Hz in a temperature range from -80 °C to 100 °C at a heating rate of 2 °C/min. Swelling force of the WSR specimen was measured with the custom-made apparatus, shown in Fig. 1, at room temperature. A WSR specimen was placed between a pair of porous stones in a cylinder, which was immersed in distilled water, and the swelling force of the WSR specimen was monitored by a load cell (TR22S-500N, Sohgoh Keiso, Tokyo, Japan) under isochoric conditions.

RESULTS AND DISCUSSION

The nominal stress–strain curves of the WSR specimens are shown in Fig. 2. The addition of SAP results in a significant increase of the Young's modulus and yield stress as listed in Table 2, proving that the reinforcement effects were present. The true stress is plotted against the Gaussian strain in Fig. 3. The WSR showed typical rubber elasticity, and the modulus G obviously increases with the concentration of SAP. The steep slopes, which occurred when SAP concentrations were high, are explained by the increase of the network density $\nu = G/k_BT$ (Table 1), where k_B and T are the Boltzmann constant and temperature, respectively.

The dynamic mechanical spectra of the WSR are shown in Fig. 4. The storage modulus (E') of the butyl rubber gradually decreases above -66 °C, and the loss modulus (E'') shows a peak at around -65°C due to the glass transition.[20] For the CR matrix, similar behaviors are observed

in the glass transition region, at T_g ≈ -40 °C.[21,22] The dynamic mechanical spectra of WSR show gradual vertical shifts from the addition of SAP, with maintaining the overall behavior of E' and E'', suggesting reinforce effects by the SAP, as observed in the tensile tests.

Vertical shifts of the dynamic mechanical spectra by the reference to the storage modulus of neat rubber give master curves shown in Fig. 5. The shift factors b_ϕ for butyl as well as the CR matrices are plotted against the volume fraction, ϕ, of the SAP in Fig. 6. It is found that the shift factors for butyl and CR lie on a single curve. The shift factors in the dilute region (ϕ < 0.1) are described by the Einstein relation for the reinforcement effect by fillers in rubber:

$$b_\phi = 1 + 2.5\phi \tag{2}$$

Thus, the interaction between the SAP particles can be ignored in this dilute region. The experimental shift factors show an appreciable upper deviation from the linear relation at high SAP concentrations. The addition of a quadratic term results in the Guth-Gold equation:

$$b_\phi = 1 + 2.5\phi + 14.1\phi^2 \tag{3}$$

Eqn. (3) describes the dependence between the volume fraction with a shift factor up to 0.4, which indicates that the pair-wise interaction between the SAP particles are effective in the semi-dilute region. Although the overall volume fraction dependence is reproduced by eqn. (3), the modified Guth-Gold equation can be expressed by:

$$b_\phi = 1 + 0.67f\phi + 1.62f^2\phi^2 \tag{4}$$

Eqn. (4) generate more accurate predictions than those of eqn. (3) for the shift factors up to ϕ=0.3 by assuming an aspect ratio of f=2.7. At higher SAP contents, Halpin-Tsai equation (5) can be applied, in which the randomly dense-packing of filler particles is assumed:

$$b_\phi = \frac{1+AB\phi}{1-B\Psi\phi}, \tag{5}$$

where constants *A*, *B*, and Ψ can be calculated by Eqns. (6), (7), and (8), respectively:

$$A = \frac{7-5\nu_1}{8-10\nu_1} \tag{6}$$

$$B = \frac{b_\phi - 1}{b_\phi + A} \tag{7}$$

$$\Psi = 1 + \left(\frac{1-\phi_m}{{\phi_m}^2}\right)\phi \tag{8}$$

and ν_1 = 0.5 is the Poisson ratio of the matrix. The maximum packing fraction ϕ_m is estimated to be approximately 0.60, similar to the value for random packing (0.637).

The microscopic images of SAP particles and the cross section of the WSR specimen are shown in Figs. 7 and 8, respectively. The average size of the SAP is ≈30 μm, and the aspect ratio shows no deviation from one, whereas the modified Guth-Gold analysis suggests that the aspect ratio of the filler is 2.7. It is noticeable, therefore, that the SAP particles are dispersed in the rubber matrix as agglomerates.

The upper deviation of the elastic moduli from the predicted curve above ϕ > 0.3 can be understood by the formation of the percolated network, caused by the interaction between the SAP particles. Furthermore, these mechanical behaviors are not affected by the matrix and that these interpretations are in good agreement with the morphology observed by the microscope (Fig. 8).

A typical result of the temporal changes of the swelling force of the WSR is shown in Fig. 9. It rapidly increases in the first 60 min, followed by a gradual increase until the end of the experiment. The time evolution of the swelling force of the WSR specimens with various thickness and diameter is shown in Figs. 10 and 11, respectively. It was found that the swelling force is essentially independent of the thickness, whereas it shows drastic increase with the diameter of the sample. In addition, as the thickness of the WSR specimen is substantially

smaller than its diameter, these results suggest that the surface area of WSR affects the swelling force.

The additional effect of the SAP is shown in Fig. 12. The swelling force curve shifts upwards with as the volume fraction of SAP increases up to 0.21, which indicates that the amount of SAP on the surface of the WSR specimen is responsible for the swelling force. If we assume that the SAP particles are uniformly dispersed in the WSR, we can consider that the amount of SAP particles in the surface layer is proportional to the volume of the surface layer:

$$w_s = w_0 \cdot \frac{V_s}{V_0} \tag{9}$$

Here *w* and *V* represents the weight of SAP and the volume of WSR, and the subscripts S and 0 denote the surface layer and the entire WSR specimen, respectively. If the thickness of the surface layer is approximated by the average diameter of the SAP particle (=30 μm), the weight of the SAP particles in the surface layer can be estimated with eqn. (9).

The swelling force divided by the weight of the surface SAP particles is shown in Fig. 13. It was observed that the swelling force curves can essentially be represented by a single curve, irrespective of the shape of the WSR specimen and with the SAP content up to 0.21. This suggests that the SAP particles on the surface layer majorly affects the swelling force. At high particles content (ϕ =0.31), the swelling force shows upper deviation (especially later than 10 min). This behavior is comprehended by considering that percolated network of the SAP particles was formed and that the penetration of water was promoted by the network. This explanation is conformed as the moduli of WSR is represented by the modified Guth-Gold equation in eqn. (4), where high aspect ratio, owing to the agglomeration of the SAP particles, is suggested.

Rhodamine 6G was used as the fluorescence probe to enable us to visualize the penetration of water into the WSR. Fig. 14 shows the cross section of the WSR specimens that were immersed in the aqueous solution of Rhodamine 6G. No penetration of water into the internal portion of the samples was observed for WSR confined in the piston. When the WSR was soaked without confinement, however, the water deeply penetrated into the specimen. The SAP particles on the surface of the WSR specimen, therefore, contribute to the swelling force and that the swelling behavior is substantially affected by the environment of the WSR.

The swelling force normalized by the weight of the surface SAP particles for the CR matrix is shown in Fig. 15. The swelling behavior of the WSR with the CR matrix is essentially the same as that with butyl rubber. The curves for ϕ=0.11 and 0.20 agree well, suggesting that the SAP particles on the surface are responsible for the swelling of WSR. Furthermore, the upper deviation of the swelling force, for ϕ=0.27, is explained by the contribution of the SAP particles embedded in the CR matrix.

The swelling force at 60 min is plotted against w_s in Fig. 16. It is found that the swelling force F_{60} at 60 min and for ϕ < 0.25 is represented by single line. F_{60} is, therefore, empirically described as:

$$\log F_{60} \propto 0.26 w_s. \tag{10}$$

It should be emphasized that this empirical relation is applicable for every WSR, irrespective of the shape, and at a SAP content bellow 0.25 and the matrix rubber. Thus, eqn. (10) is useful to predict the swelling force and the material design of the WSR. At higher SAP contents (ϕ > 0.25), the experimental F_{60} exceeds the empirically predicted values, suggesting that the swelling occurs not only from surface layer, but also from the internal area.

CONCLUSIONS

WSR was fabricated by kneading of the SAP particles into butyl or chloroprene rubbers. The mechanical properties and the swelling behavior of WSR confined in a cylindrical geometry were investigated. The increase of the stress level is explained by the reinforcement effect of the SAP particles. The dynamic mechanical spectra of the WSR were scaled by vertical shifts. The shift factor is represented by the modified Guth-Gold and Halpin-Tsai equations below and above $\phi \approx 0.30$, respectively. The crossover from the semi-dilute to high-concentration regions is understood by the network formation between the SAP particles. It is suggested that the swelling force of the WSR under confinement is explained by the amount of the SAP particles reside in the surface layer of the WSR up to the semi-dilute region. The prediction of the swelling force, based on the SAP contents, is useful for materials and geometrical design of sealants and caulks.

REFERENCES AND NOTES

1. Polgar, L. M.; Fallani, F.; Cuijpers, J.; Raffa, P.; Broekhuis, A. A.; Van Duin, M.; Picchioni, F. *Rev. Chem. Eng.* **2019**, 35, 45-72.
2. Wang, G.; Li, M.; Chen, X. *J. Appl. Polym. Sci.* **1998**, 68, 1219-1225.
3. Wang, G.; Li, M.; Chen, X. *J. Appl. Polym. Sci.* **1999**, 72, 577-584.
4. Wang, C.; Zhang, G.; Dong, Y.; Chen, X.; Tan, H. *J. Appl. Polym. Sci.* **2002**, 86, 3120-3125.
5. Park, J. H.; Kim, D. *J. Appl. Polym. Sci.* **2001**, 80, 115-121.
6. Zhang, Z.; Zhang, G.; Li, D.; Liu, Z.; Chen, X. *J. Appl. Polym. Sci.* **1999**, 74, 3145-3152.
7. Zhang, Z.; Zhang, G.; Wang, C.; Liu, D.; Liu, Z.; Chen, X. *J. Appl. Polym. Sci.* **2001**, 79, 2509-2516.
8. Zhang, Z.; Zhang, G.; Zhang, Y.; Wang, Z.; Yu, D.; Hu, X.; Hu, C.; Tang, X. *Polym. Eng. Sci.* **2004**, 44, 72-78.
9. Sun, X.; Zhang, G.; Shi, Q.; Tang, B.; Wu, Z. *J. Appl. Polym. Sci.* **2002**, 86, 3712-3717.
10. Zhang, S. T. *Plast. Rubber Compos.* **2012**, 41, 326-331.

11. Dehbari, N.; Tang, Y. *J. Appl. Polym. Sci.* **2015**, 132, 42786.

12. Buchholz, F. L. *J. Chem. Edu.* **1996**, 73, 512-515.

13. Zohuriaan-Mehr, M. J.; Kabiri, K. *Iran. Polym. J.* **2008**, 17, 451-477.

14. Inazumi, S.; Wakatsuki, T.; Kobayashi, M.; Kimura, M. *Environ. Eng. Res.* **2007**, 44, 463-469.

15. Inazumi, S.; Kimura, M.; Wakatsuki, T.; Kobayashi, M. *J. Soc. Mater. Sci., Jpn.* **2011**, 60, 240-244.

16. Inazumi, S.; Wakatsuki, T.; Kato, K.; Kobayashi, M. *J. Soc. Mater. Sci., Jpn.* **2012**, 61, 37-40.

17. Liu, C.; Ding, J.; Zhou, L.; Chen, S. *J. Appl. Polym. Sci*. **2006**, 102, 1489-1496.

18. Saijun, D.; Nakason, C.; Kaesaman, A.; Klinpituksa, P. Songklanakarin *J. Sci. Technol.* **2009**, 31, 561-565.

19. Ogawa, I.; Yamano, H.; Miyagawa, K. *J. Appl. Polym. Sci.* **1993**, 47, 217-222.

20. Wu, J.; Huang, G.; Wang, X.; He, X.; Lei, H. *J. Polym. Sci. B* **2010**, 48, 2165-2172.

21. Bhowmick, T.; Pattanayak, S. *Cryogenics* **1990**, 30, 116-121.

22. Kundu, P. P.; Tripathy, D. K.; Banerjee, S. *Polymer* **1996**, 37, 2423-2431.

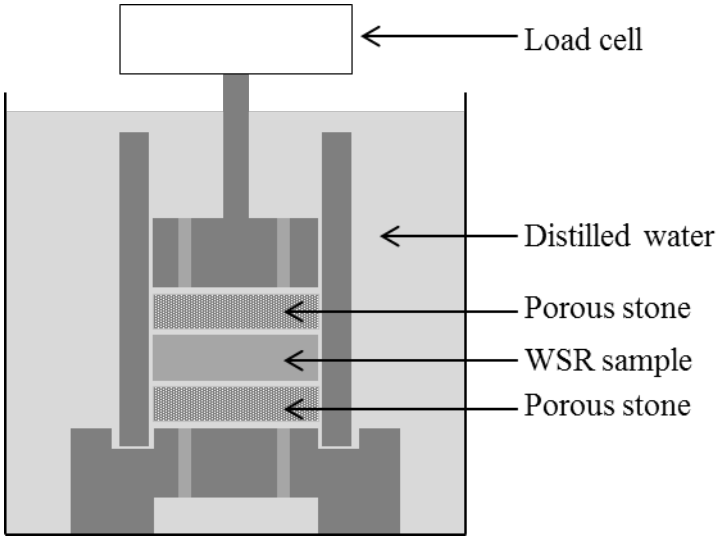

FIGURE 1 Schematic of the apparatus for measurements of the swelling force.

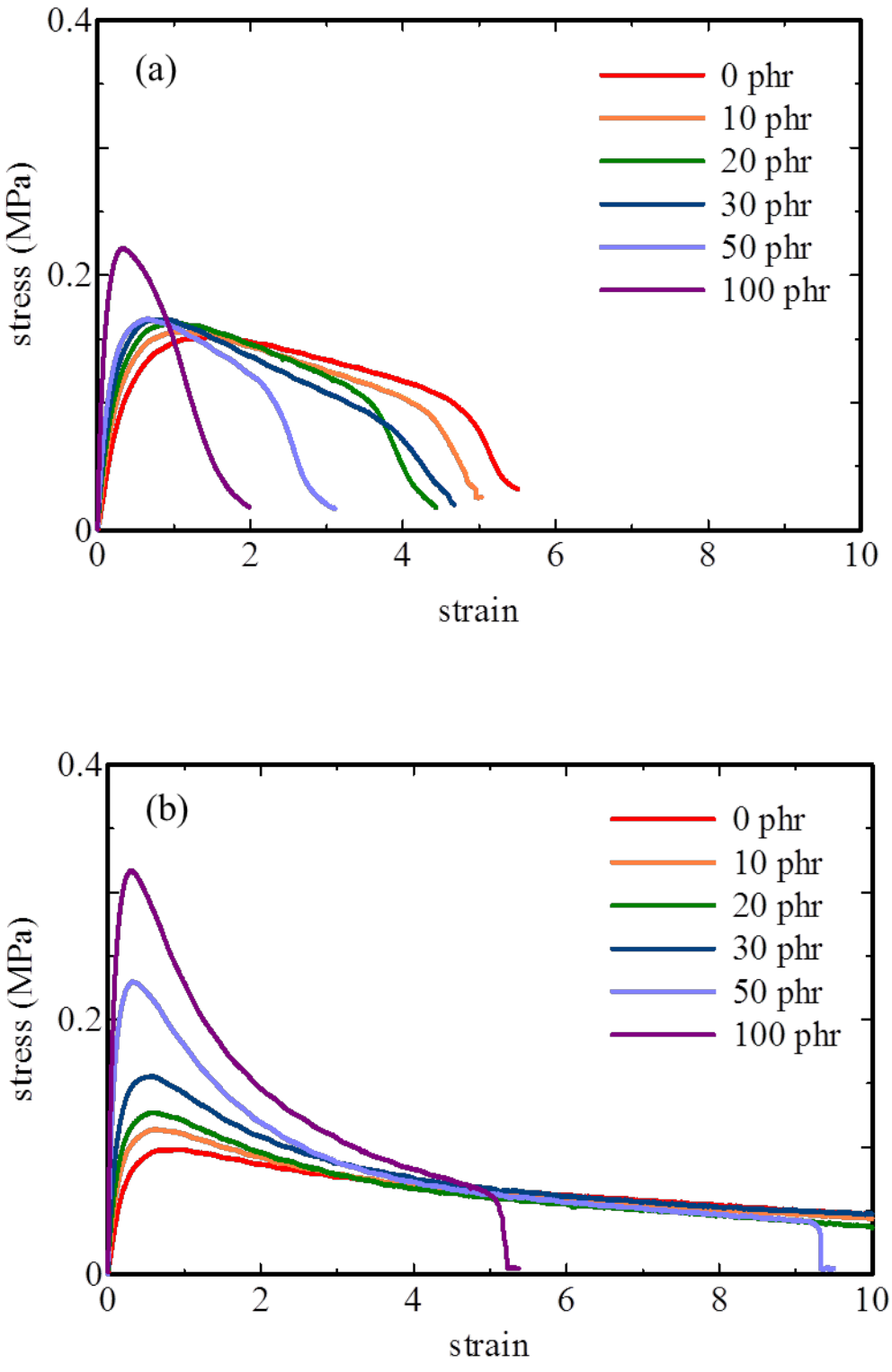

FIGURE 2 Stress–strain curves of (a) WSR (butyl + SAP) and (b) WSR (CR + SAP) for various SAP contents.

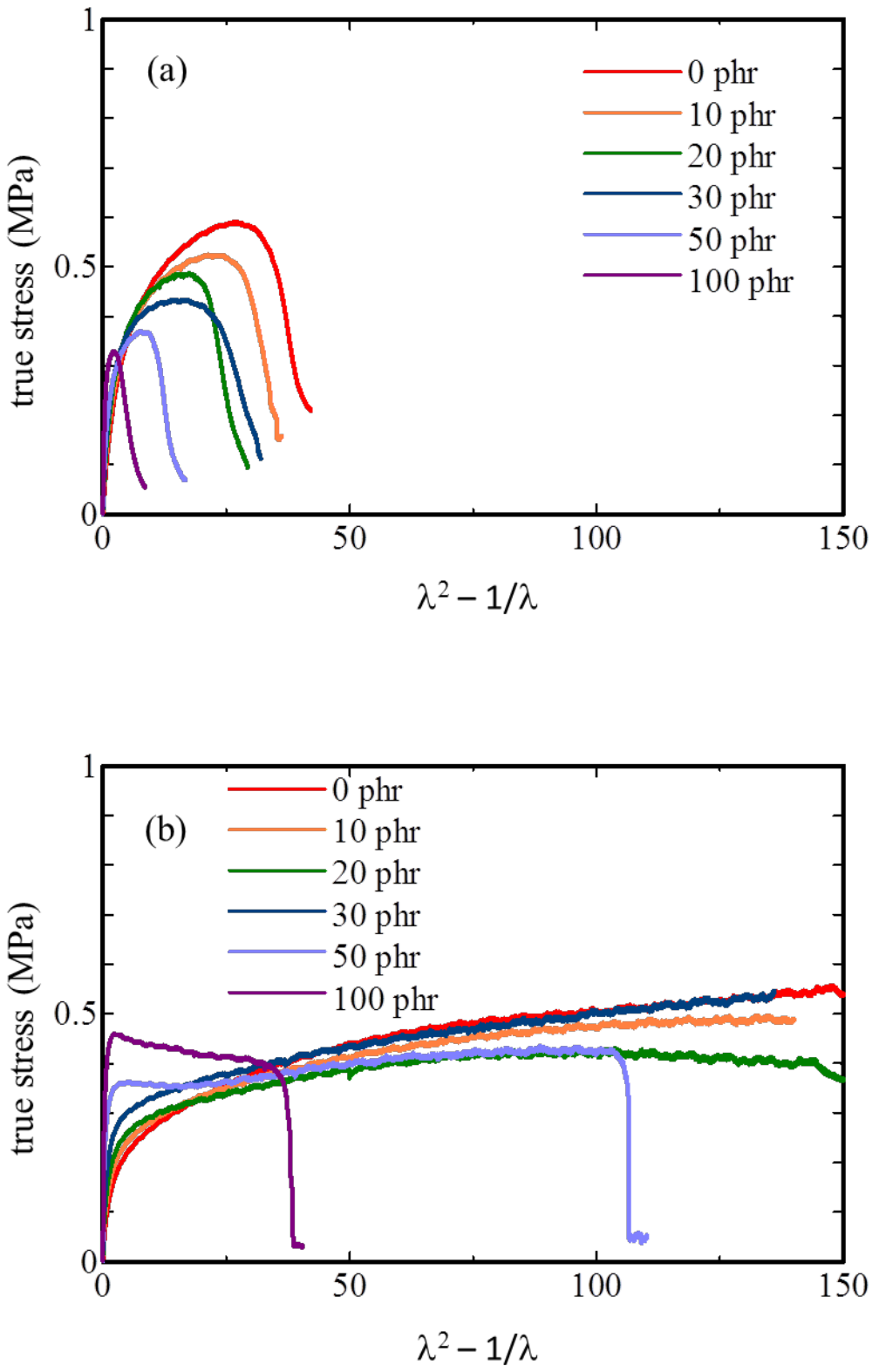

FIGURE 3 Gaussian plots of (a) WSR (butyl + SAP) and (b) WSR (CR + SAP) for various SAP contents.

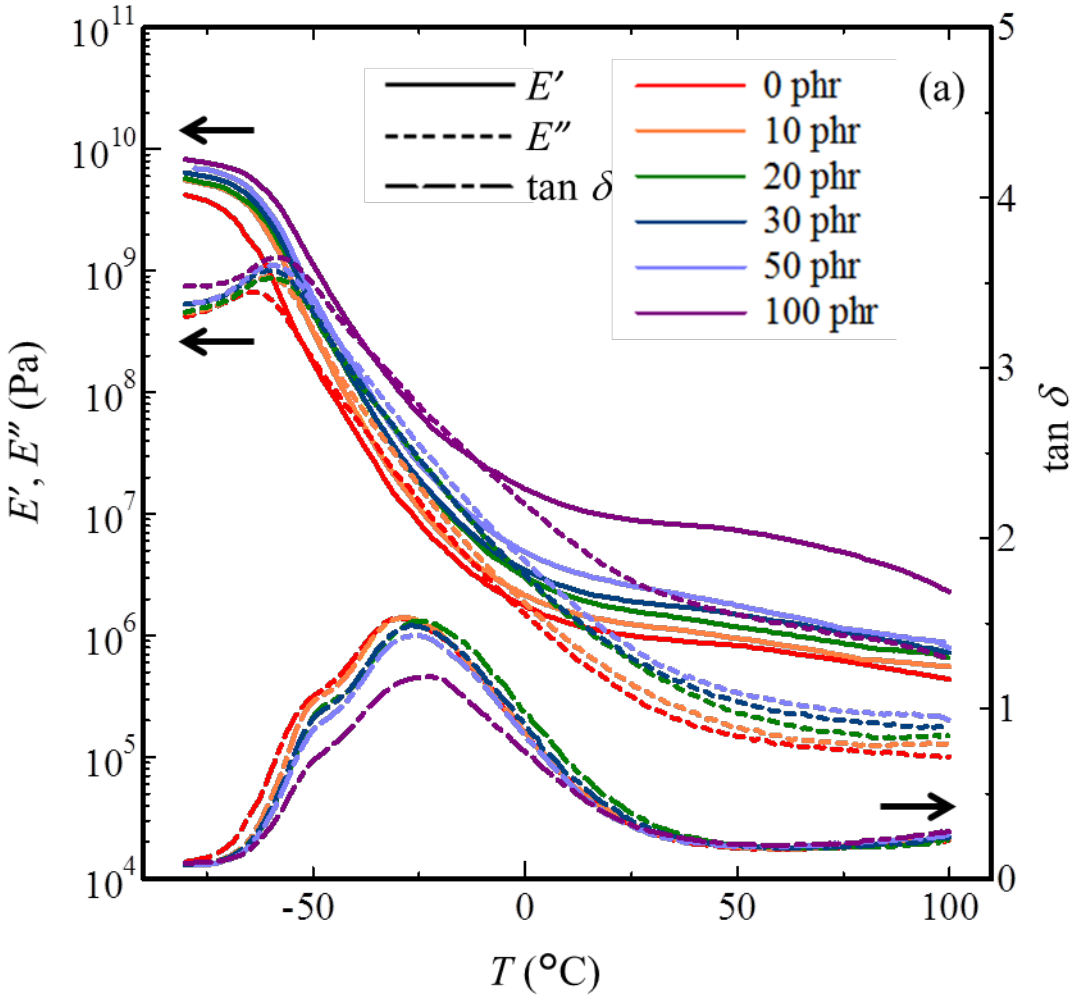

FIGURE 4 DMA spectra of WSR with (a) butyl and (b) CR rubbers for various SAP contents.

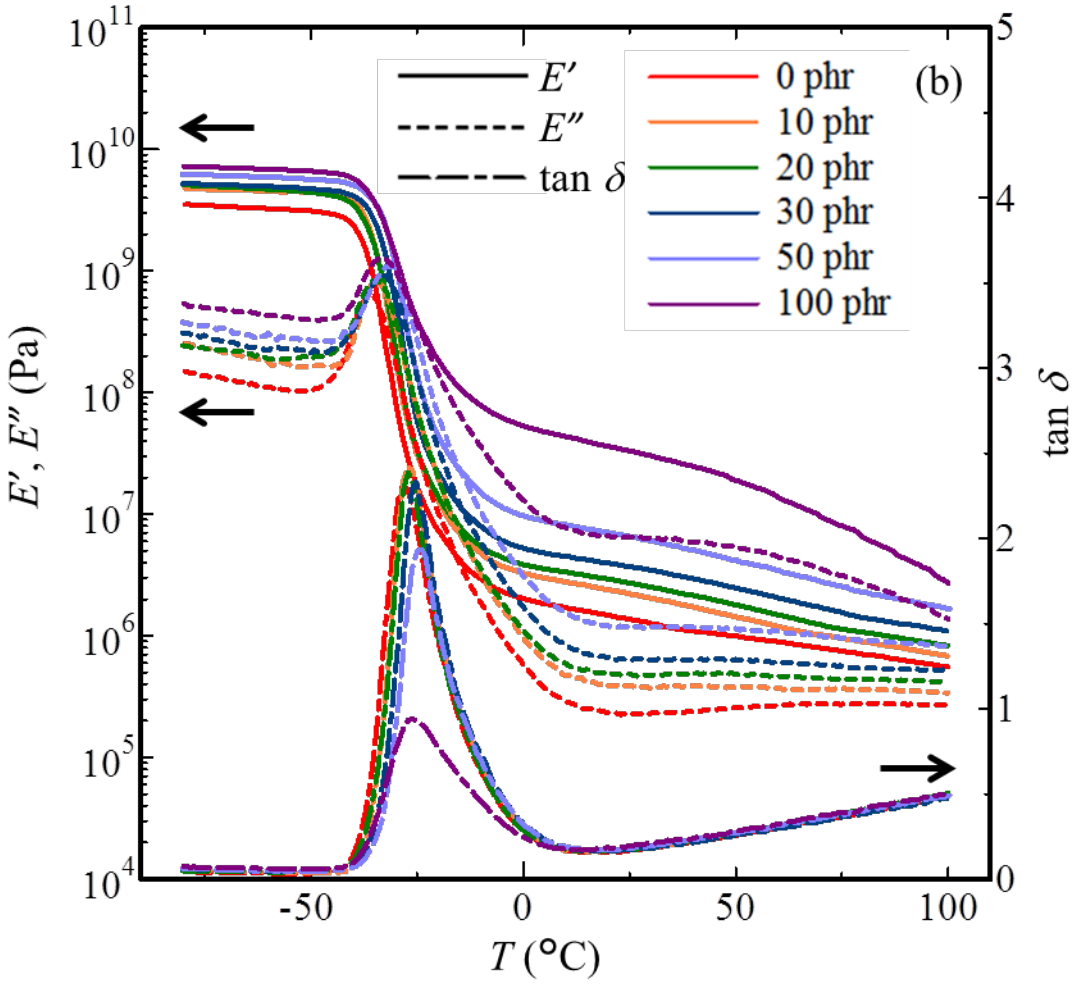

FIGURE 4 (continued) DMA spectra of WSR with (a) butyl and (b) CR rubbers for various SAP contents.

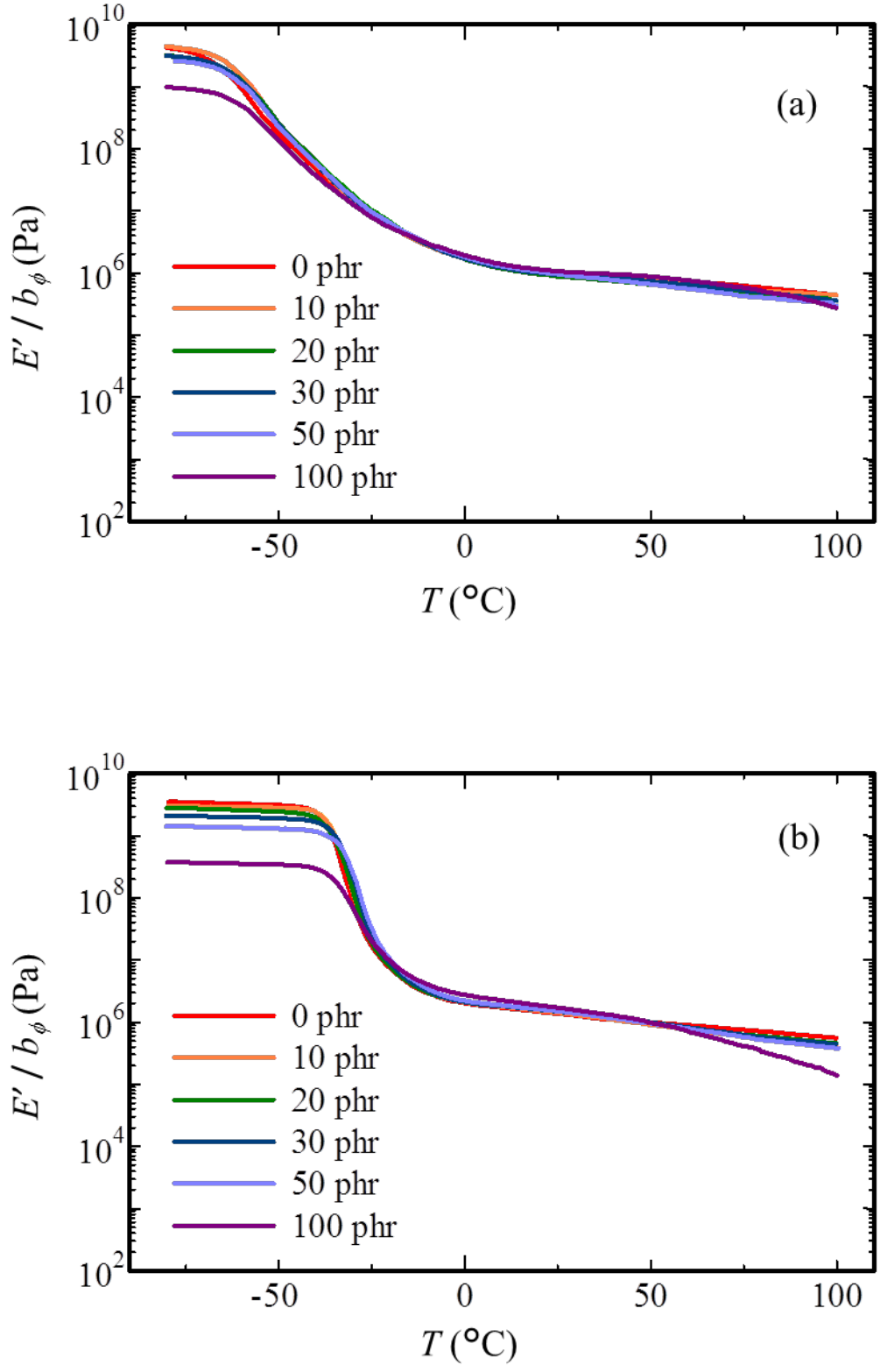

FIGURE 5 Vertically shifted storage modulus curves of WSR with (a) butyl and (b) CR rubbers.

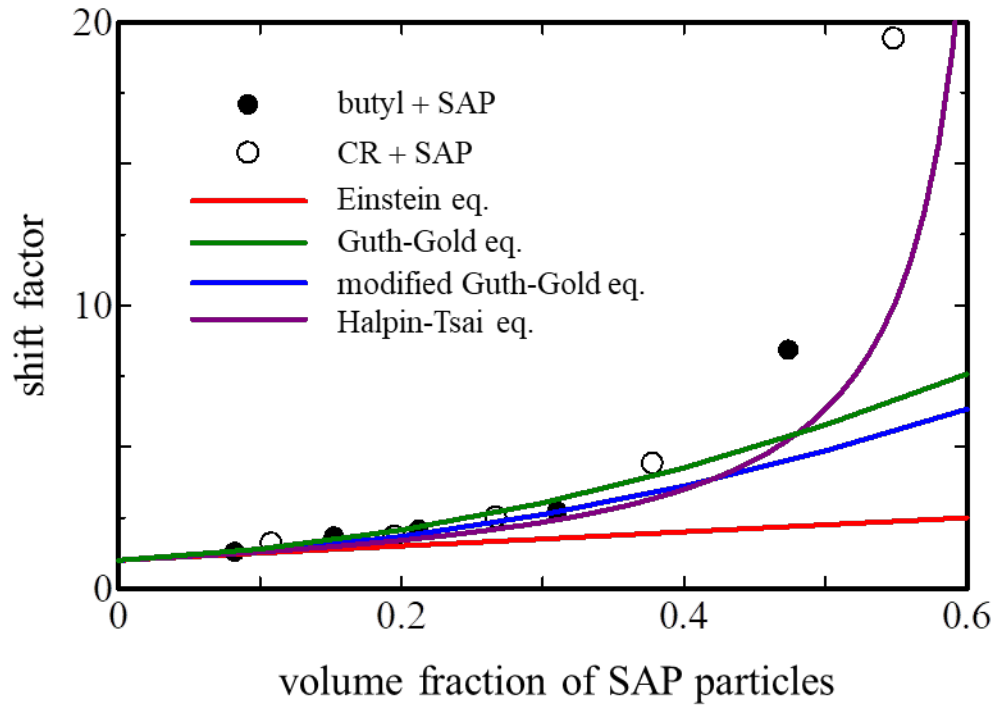

FIGURE 6 Shift factor of WSR with butyl (closed) and CR (open) rubbers plotted against the volume fraction of SAP. The lines are calculated by theoretical and empirical equations, eqns. (2)-(8).

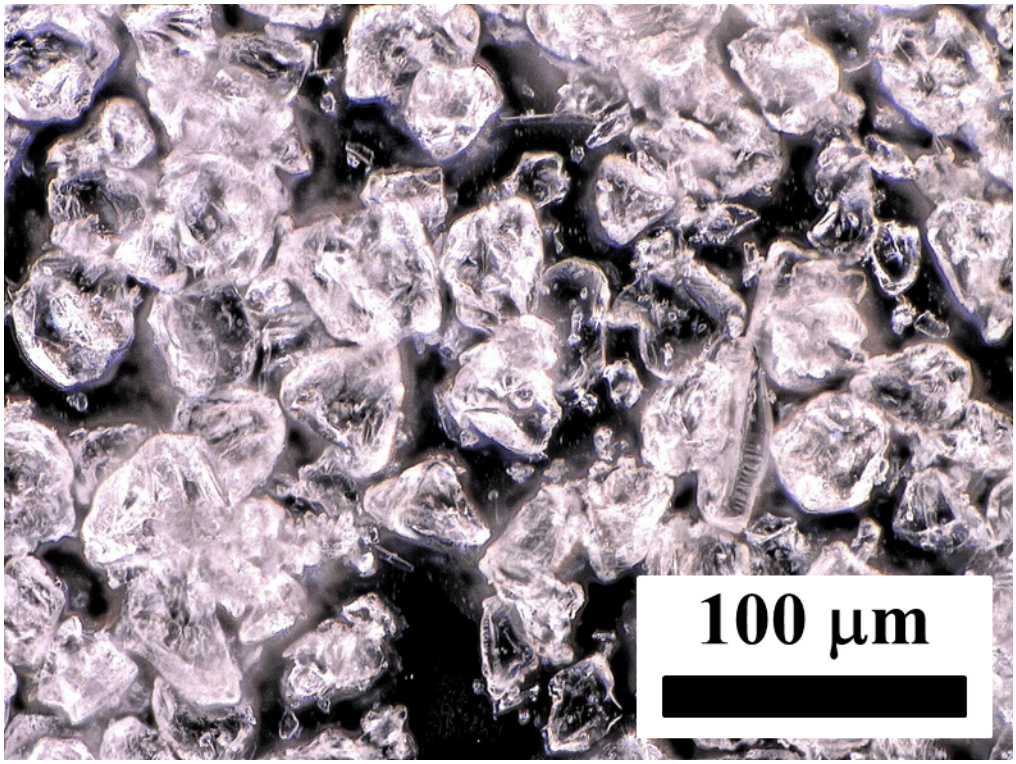

FIGURE 7 Microscopic image of the SAP particles.

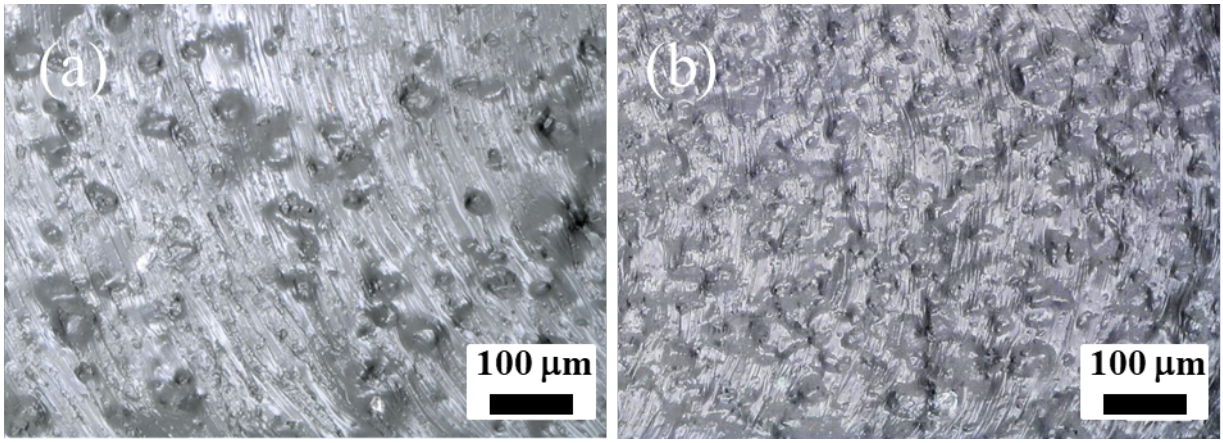

FIGURE 8 Microscopic images of cross section of WSR (butyl) with ϕ = (a) 0.08 and (b) 0.21.

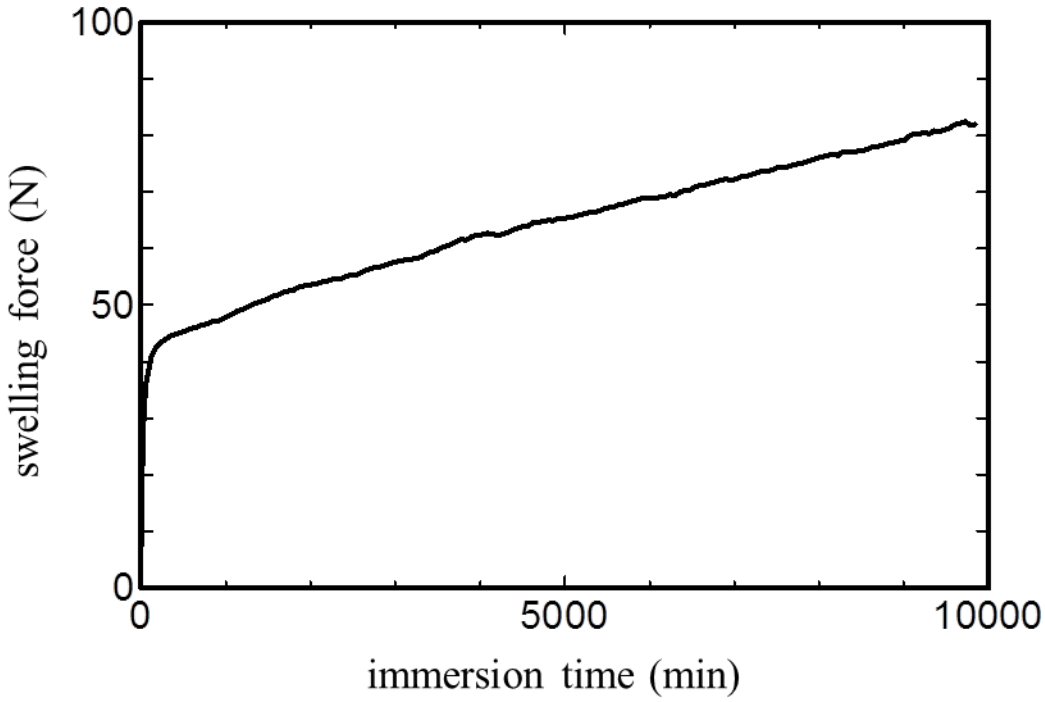

FIGURE 9 Time evolution of the swelling force of the WSR (butyl) specimen. The volume fraction of SAP is 0.21 and the specimen diameter and thickness are 30 and 1.0 mm, respectively.

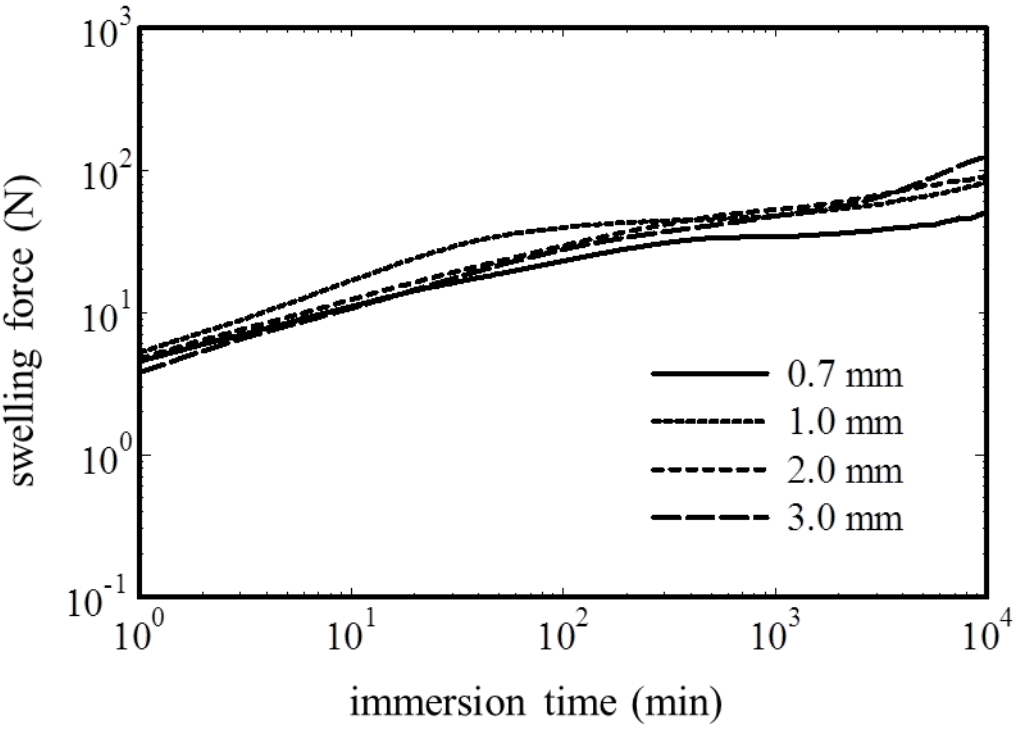

FIGURE 10 Time evolution of the swelling force of the WSR (butyl) for specimens with various thicknesses. Its volume fraction of SAP is 0.21 and the specimen diameter is 30 mm.

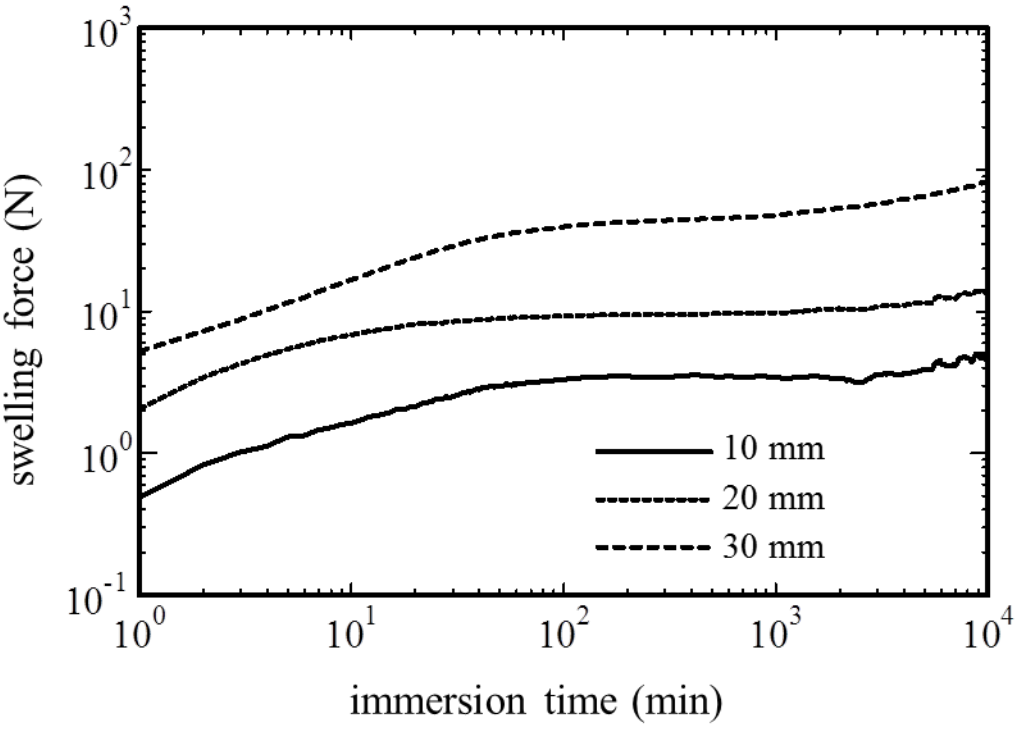

FIGURE 11 Time evolution of the swelling force of the WSR (butyl) specimens with various diameters. The thickness is 1.0 mm, and the volume fraction of the SAP is 0.21.

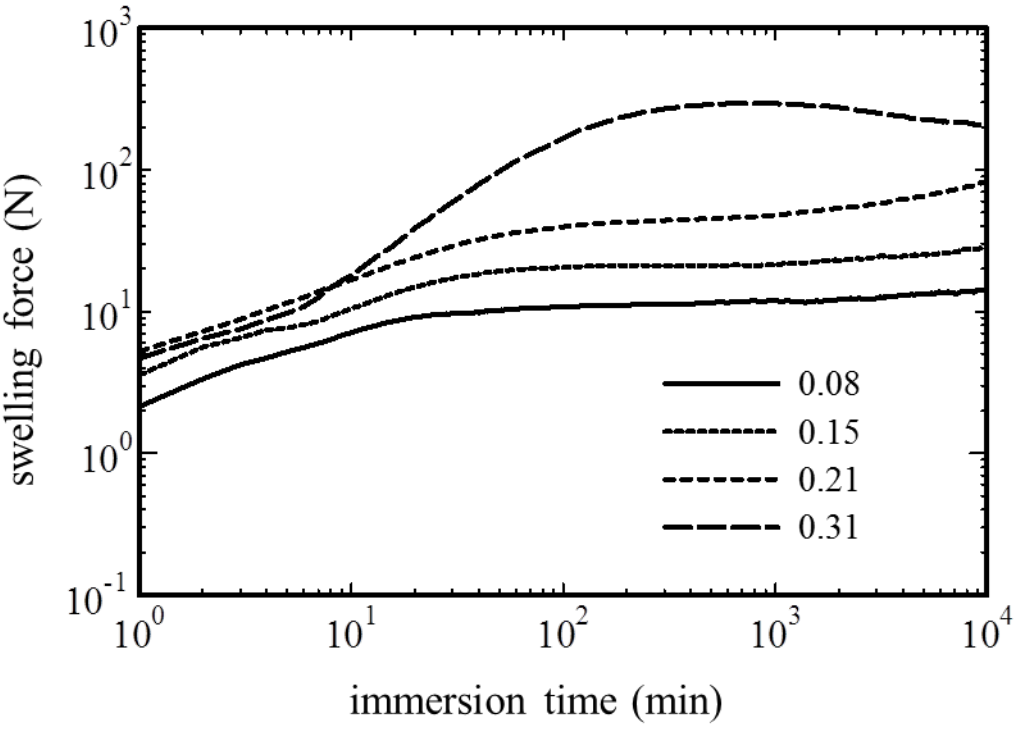

FIGURE 12 Time evolution of the swelling force of WSR (butyl) for various SAP contents. The diameter and the thickness the WSR specimen are 30 and 1.0 mm, respectively.

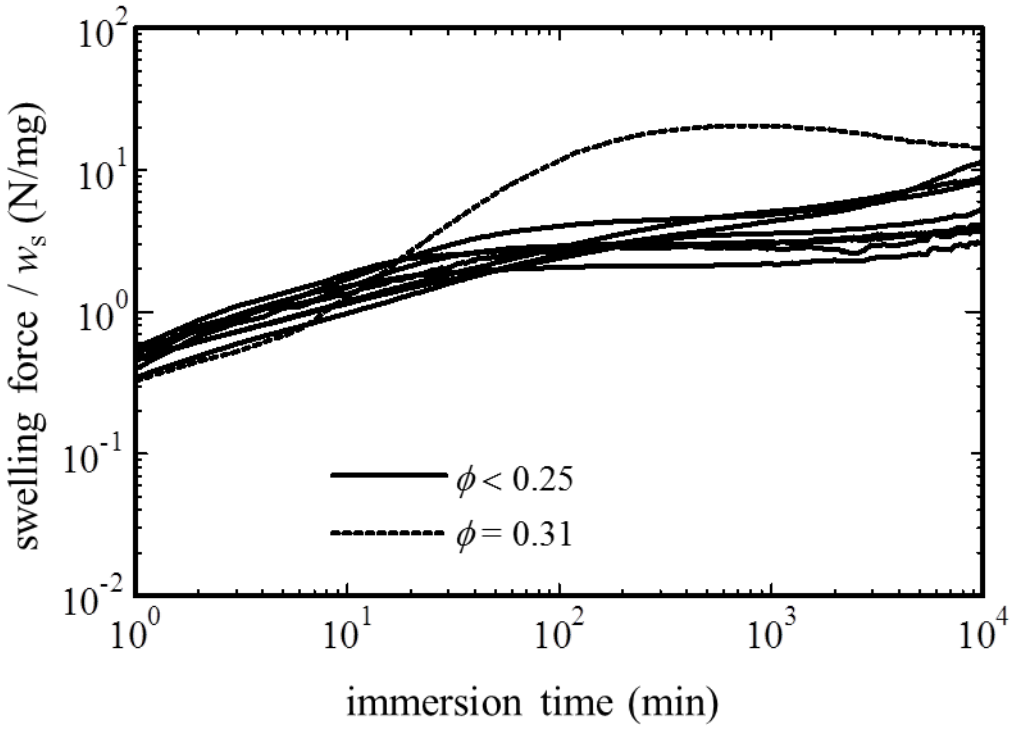

FIGURE 13 Swelling force normalized by w_s plotted against immersion time for WSR (butyl) with various diameter and thickness. The solid and dotted lines represent WSR with ϕ < 0.25 and ϕ = 0.31, respectively.

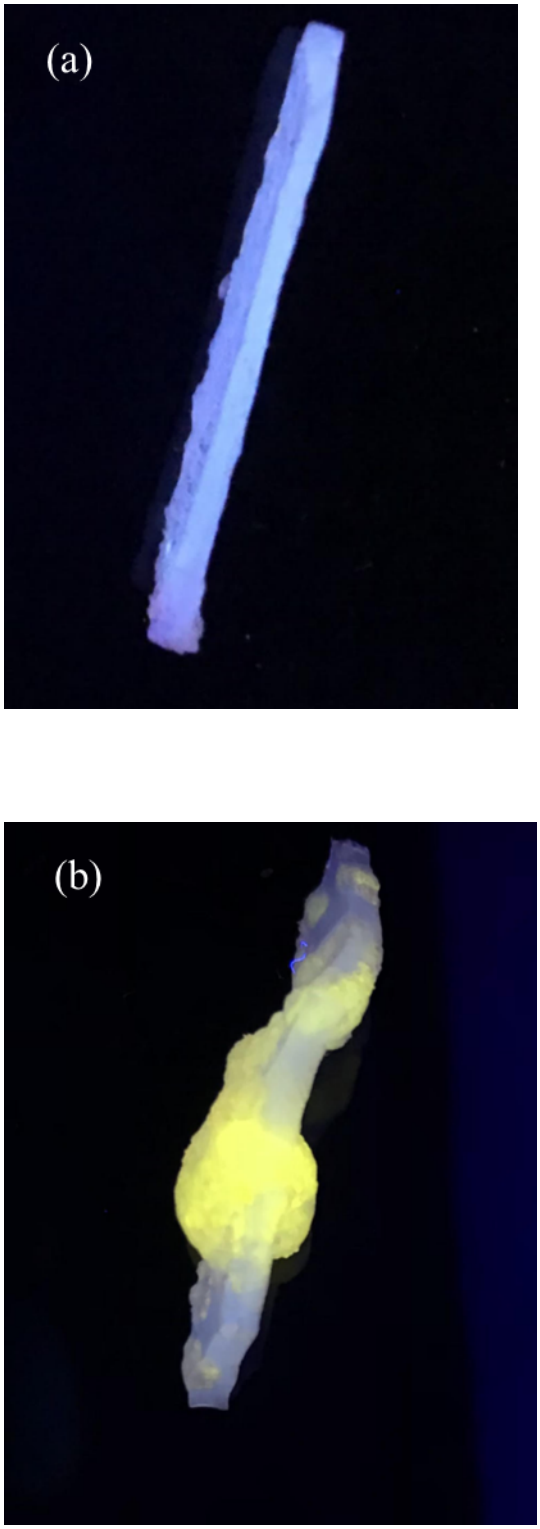

FIGURE 14 Microscopic images of cross section of WSR (butyl rubber, $\phi = 0.21$) after the immersion in aqueous solution of Rhodamine 6G for 14 days (a) with and (b) without cylindrical confinement.

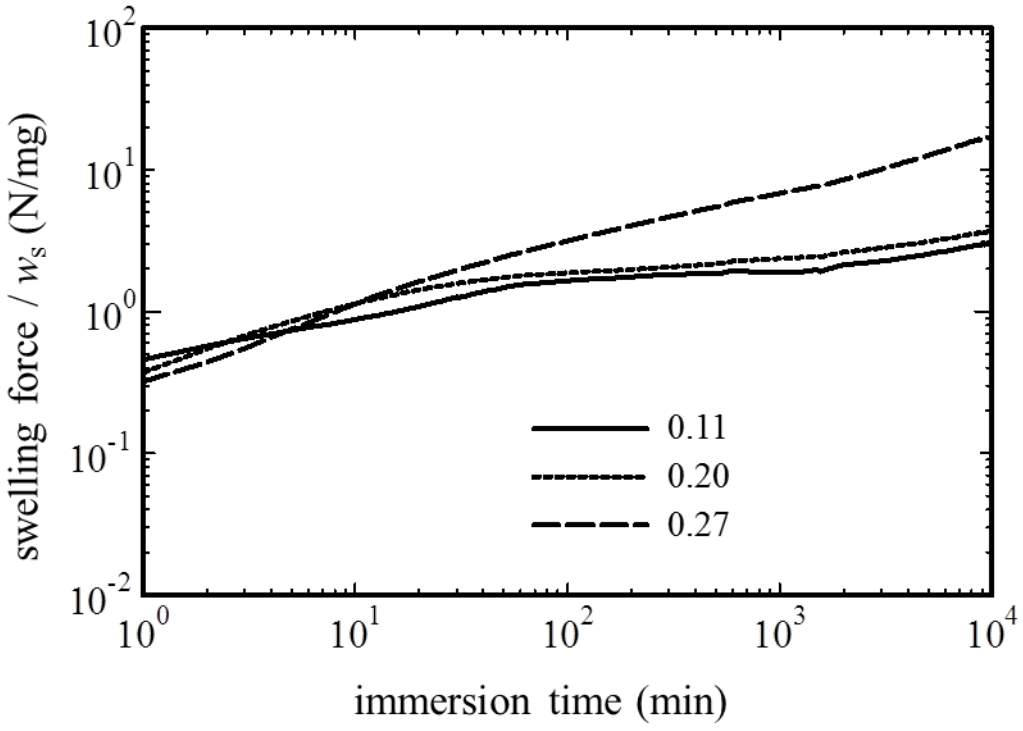

FIGURE 15 Effect of the SAP volume fraction on the normalized swelling force of WSR (CR + SAP) with specimen diameter of 30 mm and thickness of 1.0 mm.

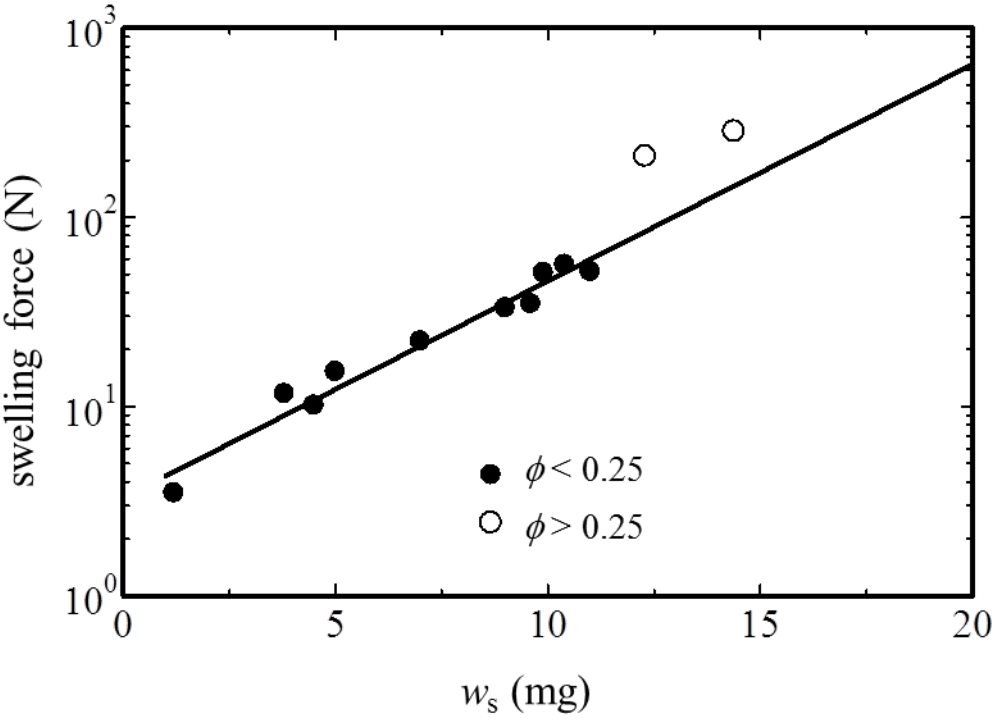

FIGURE 16 Swelling force after immersion in water for 60 min against the weight of SAP on the surface for various WSR specimens.

TABLE 1 Characteristics of WSR specimens.

rubber	SAP		WSR specimen		w_s [mg]
	content [phr]	volume fraction	diameter [mm]	thickness [mm]	
butyl	10	0.08	30	1.0	3.8
	20	0.15	30	1.0	7.0
	30	0.21	10	1.0	1.2
			20	1.0	4.5
			30	0.7	9.6
			30	1.0	9.9
			30	2.0	10.4
			30	3.0	11.0
	50	0.31	30	1.0	14.4
CR	10	0.11	30	1.0	5.0
	20	0.2	30	1.0	9.0
	30	0.27	30	1.0	12.3

TABLE 2 Characteristics of WSRs (butyl + SAP and CR + SAP).

rubber	SAP content (phr)	Young's modulus (MPa)	Maximum stress (MPa)	Network density ($\times 10^{19}$ m^{-3})
butyl	0	0.516	0.151	3.52
	10	0.645	0.155	4.41
	20	0.664	0.164	4.50
	30	0.724	0.164	5.05
	50	0.848	0.163	5.63
	100	1.607	0.222	8.78
CR	0	0.436	0.099	3.30
	10	0.627	0.114	3.98
	20	0.746	0.126	4.37
	30	0.959	0.155	5.46
	50	1.755	0.226	8.71
	100	2.531	0.314	12.20

GRAPHICAL ABSTRACT